DESIGN OF A SAMPLE COOLER WITH MINIMIZED PRESSURE DROP AND HIGH COOLING EFFICIENCY

MIROSLAV RIMAR[1], JAN KIZEK[1], PETER ORAVEC[1], MARCEL FEDAK[1], WOJCIECH BIALIK[2], LEONID GRES[3]

[1]Technical University of Kosice, Faculty of Manufacturing Technologies with a seat in Presov, Presov, Slovak Republic

[2]Silesian University of Technology, Faculty of Materials Engineering, Katowice, Poland

[3]Ukrainian State University of Science and Technologies, Dnipro Metallurgical Institute, Dnipro, Ukraine

DOI: 10.17973/MMSJ.2026_06_2026010

jan.kizek@tuke.sk

This paper addresses the design and thermal–hydraulic analysis of a heat exchanger designed for cooling sampled process air from a fermenter prior to its transport to a mass spectrometric analyzer. Due to the high humidity of the sampled air, effective cooling is required to prevent unwanted condensation during transport over a distance of 200 m.

A tube-in-tube counter-current heat exchanger was selected and analyzed with respect to heat transfer, condensate formation, cooling water demand, and pressure losses. The results show that the proposed design achieves the required outlet air temperature with a minimal heat transfer area and acceptable hydraulic losses. Although the amount of condensate is low, periodic purging of the air-side tube is recommended to prevent a reduction in heat transfer efficiency.

The proposed solution provides a reliable and efficient method for conditioning humid process air in fermenter monitoring applications.

KEYWORDS

Airlift fermenter, cooler, SIMAX tube, moisture, pressure loss, heat exchanger

1 INTRODUCTION

In many technological processes, it is essential to ensure precisely defined and controllable operating conditions that enable effective process control. Among these, efficient heat removal and maintenance of an optimal temperature play a key role in ensuring process stability and product quality [Shinde 2022]. Such requirements are typically met by fermenters or bioreactors, which provide a controlled environment for microbial or cell-based fermentation processes. Within these systems, key parameters such as temperature, pH, oxygen supply, and mixing intensity are regulated to optimize the production of enzymes, pharmaceuticals, and food products.

As reported in the literature [Dosaev 2025, Valdiani 2019, Gaikwad 2018, Titova 2024], bioreactors can be classified according to several criteria, including operating mode (batch, fed-batch, and continuous), mixing principle (stirred-tank reactors, airlift reactors, bubble columns, membrane bioreactors), biomass state (suspended or immobilized), and reactor volume. Special designs have also been developed for tissue cultures (e.g., rotating vessels and perfusion systems) and single-use bioreactors, which reduce the risk of contamination and simplify cleaning and sterilization procedures. The evolution of bioreactor technology from laboratory-scale devices to industrial applications highlights the importance of precise control of physicochemical parameters, which is essential for scalable biomass and metabolite production, leading to reduced operational costs and increased yields in the food, pharmaceutical, and environmental sectors [Ritonja 2021].

Airlift reactors represent a class of pneumatic bioreactors in which mixing and circulation of the culture medium are achieved by gas injection rather than mechanical agitation. Their operation is based on the density difference between the gas-enriched zone (riser) and the less aerated zone (downcomer), resulting in continuous liquid circulation within a closed loop [Chriastel 1993, Livansky 1989]. Owing to their simple construction without moving parts and the associated low shear stress, airlift reactors are particularly suitable for the cultivation of shear-sensitive cells, including animal and plant cells as well as microorganisms with fragile cell walls [Paca 1987]. Their growing importance in areas such as precision fermentation and biopharmaceutical production underlines their relevance in modern and sustainable bioprocess engineering.

Reliable monitoring and control of industrial and technological processes increasingly rely on automated measurement and sampling systems, which ensure repeatability, traceability, and compliance with legislative and normative requirements. Automated measuring systems reduce operator-dependent variability and enable continuous data acquisition under well-defined operating conditions. As highlighted by Varga [Varga 2025a], the reliability and legal validity of measured data depend not only on the performance of the analytical instruments but also on the proper design of the entire measurement chain, including sampling, sample conditioning, and data acquisition and handling systems. This topic has been further elaborated in subsequent work [Varga 2025b], where practical aspects of implementing standardized data acquisition systems in thermal and emission-related applications were analyzed in greater detail. The authors emphasize that compliance with normative requirements must be supported by appropriate technical solutions in sampling and conditioning systems, as inaccuracies introduced at this stage cannot be compensated at the level of data processing. These findings further underline the necessity of integrating reliable thermal and hydraulic design into the overall measurement chain concept.

In this context, the European standard series EN 17255 or STN EN 17255 (all four parts) [STN EN 17255-1 2020, STN EN 17255-2 2021, STN EN 17255-3 2022, STN EN 17255-4 2024] establishes comprehensive requirements for data acquisition and handling systems (DAHS), emphasizing the necessity of maintaining representative sample properties from the point of extraction to the final data evaluation. Although STN EN 17255 primarily addresses data processing, reporting, and quality assurance, its application implicitly presumes a stable and well-conditioned input signal, which can only be achieved through appropriately designed sampling and conditioning systems. Improper sample conditioning, such as uncontrolled condensation in sampling lines, may compromise data integrity and thus conflict with the fundamental principles of standardized automated measurement.

Process gases extracted from technological units are often saturated with water vapor, which may result in condensation within sampling lines and analytical equipment. Such condensation can lead to systematic measurement errors, corrosion of system components, or physical blockage of sampling pathways. Therefore, controlled cooling and effective condensate removal represent essential elements of sampling system design, ensuring that the measured signal complies with the stability and reliability requirements expected by automated

measurement and data handling systems operating in accordance with STN EN 17255.

In addition to thermal performance, the hydraulic behavior of sampling and cooling systems plays a crucial role in ensuring representative and stable gas transport. Excessive pressure losses may alter the sampling flow rate, affect analyzer response time, and potentially distort the measured composition. Recent studies dealing with thermo-hydraulic optimization of heat exchangers emphasize the importance of simultaneously evaluating flow distribution, pressure drop, and heat transfer performance in order to achieve an optimal design solution [Filo 2024]. These works demonstrate that even in compact or small-scale heat exchangers, inappropriate geometric configuration can significantly increase hydraulic resistance, leading to higher energy demand or unstable operating conditions. Therefore, the assessment of pressure losses together with cooling efficiency represents an essential part of the design of sample conditioning systems.

Beyond purely technical parameters, modern process design must also reflect environmental and economic aspects. As demonstrated by previous studies focused on integrated ecological and economic assessment of thermal and process systems [Zajemska 2011], it is not sufficient to optimize only individual operating variables such as temperature or flow rate. A comprehensive evaluation should include energy consumption, environmental impacts, and cost-related indicators in order to identify globally optimal operating conditions. Such an approach enables the identification of trade-offs between hydraulic losses, cooling performance, water consumption, and overall operational costs. Therefore, the design and assessment of the proposed sample cooler should be understood not only as a thermo-hydraulic task but also as part of a broader framework of sustainable and economically rational process engineering.

In this context, the present study focuses on the design of a sample gas cooler intended for use in airlift reactor applications. The composition of the withdrawn process gas is assumed based on prior analysis, while river water from the Hron River is considered as the cooling medium. The cooler is designed using borosilicate glass 3.3 SIMAX tubes [STN ISO 3585, KAVALIERGLASS 2018]. The main objective of the work is to analyze and compare co-current and counter-current cooling configurations and to evaluate the pressure drop of the proposed cooling system, with particular emphasis on ensuring reliable sample conditioning for downstream gas analysis.

The novelty and practical value of this work consist in the integrated thermo-hydraulic analysis of the sample cooler, which combines thermal sizing, condensate prediction, and gas-side pressure drop evaluation under real operating conditions of an airlift fermenter. This approach enables the determination of the optimal length of the SIMAX glass tube and provides clear recommendations for reliable long-distance transport of humid process gas to the analyzer.

2 MATERIALS AND METHODS

2.1 Airlift Fermenter

Figure 1 shows the process flow scheme of a pneumatically agitated (air-driven) fermenter equipped with an exhaust gas treatment and sampling line. The reactor is supplied with process air at the bottom, ensuring gas–liquid mass transfer and internal circulation of the culture medium. The operating pressure inside the fermenter is controlled by a back-pressure control loop (PC) installed in the exhaust gas line, which stabilizes the internal pressure and maintains defined hydrodynamic conditions within the reactor.

The exhaust gas leaving the fermenter headspace passes through a sequence of conditioning elements. First, a defoamer section is installed to prevent liquid entrainment and foam carryover from entering the downstream equipment. Subsequently, the gas stream passes through a filter to remove aerosol particles and solid impurities, ensuring protection of analytical and conditioning components. Downstream of these elements, a dedicated sampling branch is implemented. This branch contains a sample gas cooler, highlighted in Figure 1, which represents the key component addressed in this study. The cooler is designed as a heat exchanger intended to reduce the temperature of the saturated exhaust gas stream and to induce controlled condensation of water vapor.

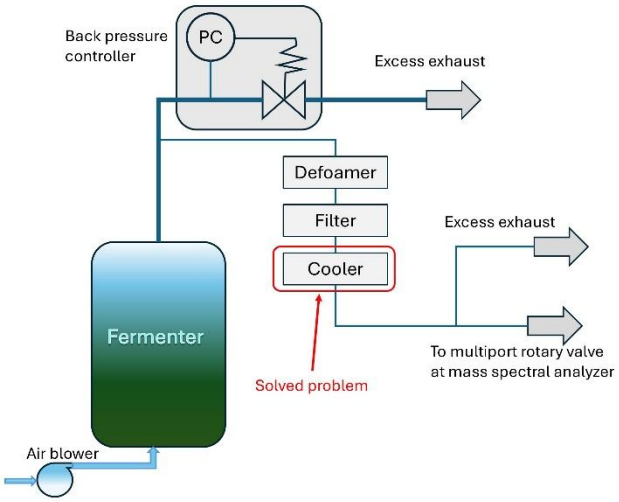

Figure 1. Process scheme of the fermenter with sampling and sample cooling

For reliable and representative gas analysis, the extracted sample must undergo thermal and phase conditioning prior to transport to the mass spectrometric analyzer. Since the exhaust gas from the fermenter is typically saturated with water vapor at operating temperature, uncontrolled cooling along the transfer line (approximately 200 m in length) would result in spontaneous condensation, leading to fluctuating sample composition, increased hydraulic resistance, and potential blockage of the sampling line. The design of the sample cooler therefore aims to achieve controlled pre-condensation of moisture at a defined temperature level.

Table 1. Input parameters of media for the sample cooler design

Parameter	Value / Range
Air from fermenter	
Inlet pressure to cooler	50 – 150 kPa
Cooler inlet air temperature	30 – 37 °C
Air saturation – relative humidity	100 %
CO_2 content	0 – 15 vol. %
O_2 content	21 – 10 vol. %
Ammonia (NH_3) content	max. 50 ppm
Flow rate	12 – 20 l.min^{-1}
Cooling medium	
Cooling water source	Hron River
Inlet water temperature	0 – 16 °C
Economic optimum – outlet water temperature	20 °C (summer conditions)

The design calculation includes determination of the required heat duty, cooling medium flow rate, overall heat transfer

coefficient, condensate mass flow rate, and pressure drop on both the gas and coolant sides. Proper thermo-hydraulic dimensioning of the cooler is essential to ensure stable sample transport conditions, minimize pressure losses, and maintain the integrity and representativeness of the analyzed gas sample.
Table 1 presents the parameters of the media determined based on measurements and available operating data, which serve as input data for the design of the sample cooler.

2.2 SIMAX glass

The cooler material is considered to be a material with high resistance to corrosion and aggressive chemical substances. For this reason, borosilicate glass SIMAX 3.3 is proposed. The properties of this material also meet the strength requirements arising from the increased pressure of the process air drawn from the fermenter. According to [STN ISO 3585 1998, KAVALIERGLASS 2018], Table 2 presents the selected material properties of SIMAX glass.

Table 2. Selected properties of SIMAX glass

	Range	Value
Coefficient of mean linear thermal expansion α	20 °C; 300 °C	3.3±0.1×10^{-6} K^{-1}
Density ρ	20 °C	2.23±0.02 g.cm^{-3}
Mean thermal conductivity λ	20 °C to 100 °C	1.2 W.m^{-1}.K^{-1}
Mean specific heat capacity at constant pressure $\bar{c}_p$	20 °C to 100 °C	0.98×10^{3} J.kg^{-1}.K^{-1}
Transformation temperature		525±15 °C
Modul of elasticity E		64×10^{-3} MPa
Ultimate tensile strength R_m		30 to 100 MPa

The high resistance of SIMAX glass products to sudden temperature changes – thermal shock resistance – is due to a low coefficient of linear thermal expansion, a relatively low Young's modulus (E), and relatively high thermal conductivity.
During the cooling and heating of a glass product, undesirable internal stresses develop. Cracking during rapid cooling occurs when these internal stresses exceed the permissible limit. Thermal shock resistance values (Δ°C) for SIMAX glass products, depending on the wall thickness, are presented in the following Figure 2.

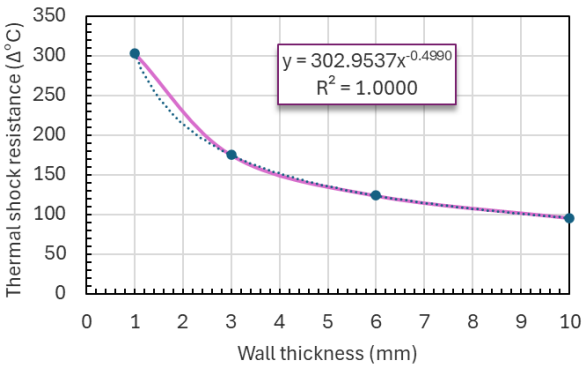

Figure 2. Thermal shock resistance of SIMAX glass as a function of wall thickness (Adapted from [KAVALIERGLASS 2018]).

Within the framework of thermal calculations, the use of a glass tube with dimensions of 8x1 mm is considered. This dimension was selected due to its high thermal shock resistance (303 °C for the given wall thickness), which represents a critical parameter for the safe operation of the designed cooler.

2.3 Computational model

The development of the computational model is based on the requirements that must be satisfied in the design of the cooler. The calculations consider the computational parameters listed in Table 3.
The thermal calculations were based on tabulated property values of the applied media as well as on developed dependency models presented in [Hasek 1980, Varga 2013, Rimar 2021]. In the case of the process air, the formation of condensate had to be taken into account, as latent heat is released during the phase change.

Table 3. Input parameters of process media for the computational model of the sample cooler

Parameter	Value / Range
Air from fermenter	
Inlet pressure to cooler p_{air}	150 kPa
Cooler inlet air temperature $t_{h,in}$	37 °C
Air saturation – relative humidity φ_{air}	100 %
CO_2 content	15 vol. %
O_2 content	10 vol. %
Ammonia (NH_3) content	max. 50 ppm
Flow rate $q_{v,air}$	12; 14; 16; 18; 20 l.min^{-1}
Cooling medium	
Cooling water source	Hron River
Inlet water temperature $t_{c,in}$	2; 5; 10; 15 °C
Economic optimum – outlet water temperature $t_{c,out}$	20 °C (summer conditions)

The calculation of the mean specific heat capacity of the gaseous components in the process air was based on a temperature-dependent correlation obtained by regression analysis of tabulated data reported in [Hasek 1980]. The regression was performed in the MS Excel software environment using a linear model over the temperature range ⟨0; 50⟩ °C.

$$c_p = a + b\,t \tag{1}$$

The coefficients a and b in Equation (1) for each gas are summarized in Table 4.

Table 4. Regression coefficients for the temperature-dependent mean specific heat capacity (kJ.m^{-3}.K^{-1}) of gaseous components

	a	b	R^2
Dry air	1.296232	2.32×10^{-4}	0.99989
Water vapor	1.482545	2.08×10^{-4}	0.99993
CO_2	1.603973	9.59×10^{-4}	0.99976
N_2	1.290432	8.0×10^{-5}	0.99990
O_2	1.288486	1.10×10^{-4}	0.99995

In the calculation of water parameters (specific heat capacity, density and Prandtl number), an effort was made to use tabulated values that exhibit local minima and local maxima within the considered temperature range. For this reason, mathematical models based on regression relationships were developed.
For the determination of the specific heat capacity of water [Raznjevic 1984], a temperature-dependent correlation

obtained by regression analysis was used. The regression was performed in the software environment SigmaPlot ver. 11, applying an Exponential Decay; Exponential Linear Combination model over the temperature range ⟨0; 50⟩ °C. The resulting regression equation is given as:

$$c_w = 4.161 + \frac{5.652}{100} e^{-\frac{7.172}{100}t} + \frac{3.637}{10^4} t \quad (2)$$

The proposed correlation exhibits a high level of agreement with reference data, achieving a coefficient of determination of R^2=0.999916. Within the analyzed temperature range, the equation shows only negligible deviations from tabulated values reported in the literature [Hasek 1980].

For the calculation of water density [Raznjevic 1984], a temperature-dependent correlation obtained by regression analysis was used. The regression was performed in the MS Excel software environment using a third-degree polynomial model over the temperature range ⟨0; 50⟩ °C. The resulting regression equation is given as:

$$\rho_w = 999.869 + \frac{53.227}{10^3} t - \frac{74.807}{10^4} t^2 + \frac{3.34}{10^5} t^3 \quad (3)$$

The presented model achieves a high level of agreement with reference values, with the correlation coefficient reaching R^2 = 0.999977. Within the analyzed temperature interval, the equation shows only negligible deviations from the tabulated values reported in the literature [Hasek 1980].

Following the previously derived temperature-dependent correlations for the thermophysical properties of water, an analogous approach was applied to determine the temperature dependence of the Prandtl number. The correlation was obtained by regression analysis of experimental (or tabulated) data using the SigmaPlot ver. 11 software, with an Exponential Decay; Exponential Linear Combination regression model applied over the temperature range ⟨0; 50⟩ °C. The resulting correlation equation is expressed as:

$$Pr_w = 4.4953 + 9.0959\, e^{-\frac{5.42}{100}t} + \frac{3.02}{10^2} t \quad (4)$$

The proposed model exhibits a high level of agreement with reference data, achieving a coefficient of determination of R^2=0.9999. Within the analyzed temperature interval, the deviations from tabulated values reported in the literature [Hasek 1980] are negligible.

Thermal calculation of the heat exchanger

The theory of heat transfer plays a significant role in engineering practice, not only from a technological but also from an energy perspective. This is due to the fact that heating and cooling of media in industrial operations consumes a substantial amount of energy [Rimar 2021].

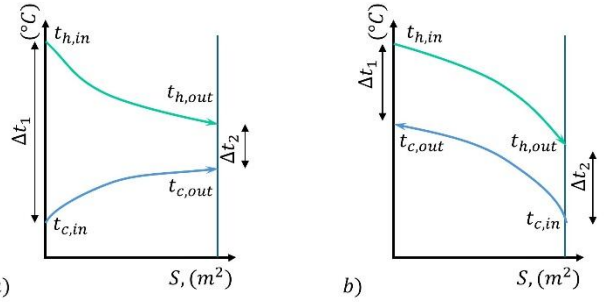

Figure 3. Temperature profiles of co-current and counter-current heat exchangers

Figure 3 illustrates the temperature profiles of heat exchangers with a) co-current and b) counter-current flow arrangements, which are used to determine the computational parameters for the thermal design of the cooler. Thus, Fig. 3 presents the temperature profiles along the heat transfer surface of a simple heat exchanger. The mean temperature difference Δt_s defined either as the arithmetic mean temperature difference or as the logarithmic mean temperature difference.

The arithmetic mean temperature difference is defined by the following relation:

$$\Delta t_s = \frac{1}{2} (\Delta t_1 - \Delta t_2) \quad (5)$$

Where $\Delta t_1$and $\Delta t_2$are determined based on Figure 3(a) or Figure 3(b), as follows:

For a co-current heat exchanger:

$$\Delta t_1 = t_{h,in} - t_{c,in}, \qquad \Delta t_2 = t_{h,out} - t_{c,out} \quad (6)$$

For a counter-current heat exchanger:

$$\Delta t_1 = t_{h,in} - t_{c,out}, \qquad \Delta t_2 = t_{h,out} - t_{c,in} \quad (7)$$

Where $t_{h,in}$ and $t_{h,out}$ denote the inlet and outlet temperatures of the hot medium, respectively, and $t_{c,in}$ and $t_{c,out}$denote the inlet and outlet temperatures of the cold medium.

If the temperatures of the media on both sides of the heat transfer surface vary only slightly, i.e. if the following condition is satisfied:

$$\frac{\Delta t_1}{\Delta t_2} \leq 1.5 \quad (8)$$

then the mean temperature difference may be approximated by the arithmetic mean temperature difference:

$$\Delta t_s = \Delta t_a = \frac{t_{h,in} - t_{h,out}}{2} - \frac{t_{c,in} - t_{c,out}}{2} \quad (9)$$

where Δt_a is the arithmetic mean temperature difference.

The logarithmic mean temperature difference is defined by the following relation:

$$\Delta t_s = \frac{\Delta t_1 - \Delta t_2}{\ln \frac{\Delta t_1}{\Delta t_2}} \quad (10)$$

According to the second law of thermodynamics, energy is transferred from the hotter flowing fluid to the colder one through the separating wall. This process represents a combination of heat transfer by convection and conduction.

In the design and calculation of heat exchangers, the amount of transferred heat Qand the required heat transfer area Sare determined. The amount of transferred heat can be obtained from the thermal balance of the device. The heat transfer area is subsequently determined using the fundamental heat transfer equation:

$$Q = k\, \Delta t_s\, S \quad (11)$$

k– overall heat transfer coefficient from one medium to the other (W.m^{-2}.K^{-1}).

The overall heat transfer coefficient can be characterized as a functional relationship:

$$k = f(\alpha_1, \lambda_i, \delta_i, \alpha_2) \quad (12)$$

For the calculation of the overall heat transfer coefficient, a cylindrical tube wall is considered, and therefore the heat transfer coefficient per unit length of the tube is determined using the following relation:

$$k_L = \frac{1}{\frac{1}{\alpha_1 d_1} + \frac{1}{2\lambda}.\ln\frac{d_2}{d_1} + \frac{1}{\alpha_2 d_2}} \quad (13)$$

α_1- heat transfer coefficient by convection from the first medium to the wall (W.m^{-2}.K^{-1}),
λ - thermal conductivity of the wall (W.m^{-1}.K^{-1}),
α_2 - heat transfer coefficient by convection from the wall to the second medium (W.m^{-2}.K^{-1}),
d_1 – outer diameter of the tube (m),
d_2– inner diameter of the tube (m).
Equations for heat transfer through a cylindrical wall:

$$Q = \pi\ L\ k_L\ \Delta t_s\ S \quad (14)$$

General heat balance equation of the heat exchanger:

$$Q_h = W_h\ c_h\ (t_{h,in} - t_{h,out}) \quad (15)$$

$$Q_c = W_c\ c_c\ (t_{c,out} - t_{c,in}) + Q_{st} \quad (16)$$

W_h, W_c - fluid flow rate (m^3.s^{-1}) or (kg.s^{-1}),
c_h, c_c mean specific heat capacity of the fluid (J.m^{-3}.K^{-1}) or (J.kg^{-1}.K^{-1}),
Q_{st} - heat losses of the heat exchanger (W).
If a phase change occurs in the heat exchanger (evaporation or condensation), the latent heat must also be taken into account in the heat balance.
The calculation of the convective heat transfer coefficients αwas based on functional relationships expressed by dimensionless correlations using the Nusselt number *Nu*. The thermophysical properties of the fluids were determined either by means of developed regression models or obtained directly from thermodynamic tables ([Hasek 1980, Raznjevic 1984]) using interpolation at the reference temperature, as described in [Rimar 2021].
For the calculation of the Nusselt number under forced turbulent flow in tubes and channels, the dimensionless correlation according to [Varga 2013, Rimar 2021] was applied:

$$Nu = 0.021\ Re^{0.8}\ Pr^{0.43}\left(\frac{Pr}{Pr_{st}}\right)^{0.25} \quad (17)$$

For gases, the Prandtl number is usually considered constant (Pr =const.), which simplifies the calculation.
For the calculation of the Nusselt number Nu for cooling water under forced laminar flow in tubes and channels, the dimensionless correlation according to [Varga 2013, Rimar 2021] was used:

$$Nu = 0.17\ Re^{0.33}\ Pr^{0.43}\ Gr^{0.1}\left(\frac{Pr}{Pr_{st}}\right)^{0.25} \quad (18)$$

The convective heat transfer coefficient αwas subsequently calculated from the obtained Nusselt number Nu using the following relationship:

$$Nu = \frac{\alpha\ l}{\lambda} \quad (19)$$

α – convective heat transfer coefficient (W.m^{-2}.K^{-1}),
l – characteristic length (m),
λ – thermal conductivity of the fluid (W.m^{-1}.K^{-1}).

Hydraulic calculation of the heat exchanger

The hydraulic calculation of heat exchangers is important primarily with respect to fluid flow on both sides of the heat transfer surface. This calculation is essential for the proper sizing of equipment ensuring fluid circulation, as well as for assessing the effect of pressure losses on the operation of the working (cooling) circuit, particularly on the function of the compressor.
When a real fluid flows through a pipeline, pressure losses occur. These losses arise due to friction between the fluid and the pipe walls (distributed pressure loss) as well as due to local resistances caused by changes in flow direction, changes in pipe cross-section, and the presence of fittings, valves, and other structural elements (local pressure loss).
Based on the pressure losses on the primary side of the heat exchanger and its connecting pipelines, it is necessary to determine the optimal pressure difference of the entire system with regard to the correct and reliable operation of control components, particularly the control valve.
The pressure loss on both the outer and inner sides of the heat transfer surface of the heat exchanger can be determined as the sum of individual resistances:

$$\Delta p_c = \sum\Delta p_\lambda + \sum\Delta p_\xi \quad (20)$$

$\sum\Delta p_\lambda$– sum of pressure losses due to fluid friction along the flow length (Pa),
$\sum\Delta p_\xi$– sum of partial local pressure losses (Pa).
The distributed pressure loss along the pipe length can be expressed using the Darcy–Weisbach equation:

$$\Delta p_\lambda = \lambda\ \frac{L}{d}\frac{\rho w^2}{2} \quad (21)$$

λ– friction factor along the pipe length, which depends on the kinematic viscosity of the fluid ν, mean flow velocity w, pipe diameter d, and the roughness of the inner pipe surface ε(expressed as relative roughness $\delta = \varepsilon/d$) (–),
L– pipe length (m),
d– inner pipe diameter (m),
ρ– density of the transported medium (kg.m^{-3}),
w– velocity of the flowing medium (m.s^{-1}).
The influence of viscosity, flow velocity, and pipe diameter on the friction factor can be expressed using the Reynolds number:

$$Re = \frac{w_t\ d}{\nu_t} \quad (22)$$

w_t– fluid velocity under given conditions (m.s^{-1}),
ν_t– kinematic viscosity of the fluid under given conditions (m^2.s^{-1}).
The hydraulic friction factor λcan be determined using empirical correlations proposed by various authors. One of the classical approaches is the classification of flow regimes according to Nikuradze, who divided the flow into five regions based on the Reynolds number Re.
Based on the performed calculations, it was found that the airflow is in the transitional flow regime. Therefore, it is sufficient to apply the following empirical correlation as presented in [Rimar 2021]:

$$\lambda = 0.1\left(\frac{1.46.\ \delta}{d} + \frac{100}{Re}\right)^{0,25} \quad (23)$$

Amount of Condensate

The mass density of water vapour in air at saturation is denoted as ρ_p''. This value increases with air temperature, since the saturation pressure p_p''also increases. The values of $p_p''$and ρ_p'' are given either in steam tables or can be expressed by functional relationships.
The amount of vapour contained in air (absolute humidity) ranges within

$$\rho_p = (0 \div 1)\, \rho_p''. \quad (24)$$

This range varies with air temperature. However, absolute humidity is not a characteristic quantity for describing air humidity, since the same amount of vapour may correspond to a superheated, undersaturated, or saturated state of air.
For the saturated state, the vapour density ρ_p'' can be calculated using the following relationship given in [Rimar 2021]:

$$\rho_p'' = \frac{217.6}{273.15 + t}\, p_p'' \quad (25)$$

Similarly, the saturation vapour pressure p_p'' can be expressed as a function of air temperature. For the temperature range <0; 80°C>, the following relationship from [Rimar 2021] can be applied:

$$\ln p_p'' = 23.58 - \frac{4044.2}{235.6 + t} \quad (26)$$

Another important air parameter is the specific humidity $x(kg.kg_{dry\ air}^{-1})$, which represents the mass of water vapour contained in moist air relative to 1 kg of dry air [Rimar 2021]:

$$x = 0.622 \frac{\varphi\, p_p''}{p - \varphi\, p_p''} \quad (27)$$

p– absolute pressure in the exchanger in/out (Pa).
The amount of condensate formed is determined from the difference in specific humidity x between the inlet and the outlet of the cooler according to the following relationship:

$$q_{m,condensate} = m, q_{dry\ air} \Delta x \quad (28)$$

$m_{dry\ air}$ is the mass flow rate of dry air and

$$\Delta x = x_{in} - x_{out} \quad (29)$$

The formation of condensate contributes to the total heat duty of the cooler through the release of latent heat. The total heat load of the exchanger is therefore expressed as the sum of sensible and latent heat components which expands equation (15):

$$Q_{total} = Q_{sens} + Q_{lat} \quad (30)$$

$$Q_{sens} = W_{gas}\, c_{p,gas}\, (T_{in} - T_{out}) \quad (31)$$

$$Q_{lat} = q_{m,cond}\, r \quad (32)$$

r- latent heat of vaporization (J.kg^{-1}),
$q_{m,cond}$ – condensate mass flow rate (kg.s^{-1}),
W_{gas} – total fluid flow rate of moist gas (m^3.s^{-1}) or (kg.s^{-1}).
Thus, the condensation process significantly affects the required heat transfer area, since the latent heat release may represent a substantial portion of the total heat duty, especially at high inlet humidity.

Computation Algorithm

The calculation algorithm was based on input parameters obtained either from thermodynamic tables [Hasek, 1980; Raznjevic, 1984] or from analytical relationships presented in [Varga, 2013; Rimar, 2021]. Where tabulated data were used, regression correlations were derived exclusively for the purposes of this study and are presented as original relationships within the text.
The computational procedure consisted of the following steps:

1. Input parameters
- Process air and cooling water operating parameters (Table 3)
- Thermophysical properties of borosilicate glass (Table 2)

2. Calculation of process air properties
- Determination of molar mass M_{air} based on gas composition (Table 3)
- Calculation of specific gas constant r_{air} and air density $\rho_{t,air}$
- Determination of Prandtl number Pr_{air} at mean air temperature
- Calculation of specific humidity x_{in}, x_{out} and condensate mass flow rate $q_{m,cond}$
- Evaluation of Reynolds number Re_{air}, Nusselt number Nu_{air} (Eq. 16), and convective heat transfer coefficient α_{air}

3. Calculation of cooling water properties
- Specific heat capacity c_w (Eq. 2)
- Density ρ_w (Eq. 3)
- Prandtl number Pr_w (Eq. 4)

4. Thermal calculation
- Heat supplied by process air Q_h (Eq. 30)
- Cooling water mass flow rate $\dot{m}_w$ from heat balance $Q_h = Q_c$
- Logarithmic mean temperature difference Δt_s (Eq. 10), determined using Eq. (7) for counter-current flow
- Overall heat transfer coefficient k_L (Eq. 13), based on calculated $Re_{air}, Pr_{air}, Nu_{air}$ (Eq. 17), Re_w, Pr_w, Gr_w, and Nu_w (Eq. 18)
- Required cooling tube length L, calculated from Eq. (14) and the heat balance condition under steady-state assumptions (no heat losses, $Q_{in} = Q_{out}$)

5. Hydraulic calculation
- Pressure losses on the cooling water side were not evaluated, as they are not directly related to the sampling process and the flow remained in the laminar regime throughout the investigated range.
- Air flow was assumed to occur in a smooth glass tube.
- Local pressure losses were neglected due to the straight tube configuration; only distributed pressure loss Δp_λ (Eq. 21) was considered.
- The friction factor λ was determined according to the flow regime based on Re_{air} (Eq. 23).

6. Parametric evaluation
Steps 2–5 were repeated for cooling water inlet temperatures $t_{c,in} \in \{2,5,10,13,15\}\,°C$ and for process air volumetric flow rates $q_{v,air} \in \{12,14,16,18,20\}\, L.min^{-1}$.

7. Output parameters
- Condensate mass flow rate $q_{m,cond}$
- Heat duty supplied by air Q_{air}
- Required cooling water mass flow rate $q_{m,w}$
- Cooling tube length L
- Distributed pressure loss Δp_λ

3 RESULTS AND DISCUSSION

The air supplied from the fermenter is assumed to be in a saturated state, and a selected design outlet temperature of the cooler is considered. Based on the chosen outlet temperature, a saturated air state is expected, which should prevent further condensate formation during the transport of the cooled sample to the analyzer. The calculations were carried out using certain simplifications and assumed parameters, which are listed in Table 3.
The relationships described in the preceding chapters were applied to the calculations of a counter-current heat exchanger designed as a cooler for process air from the fermenter. Verification calculations showed that this type of heat exchanger requires a smaller heat transfer area to achieve the required

outlet temperatures, which represents a significant advantage for the intended process air sample cooling application.

A tube-in-tube heat exchanger configuration was selected, with an outer tube diameter of 40 mm for the cooling water. Due to the low flow rates of the sampled process air, it was necessary to provide a sufficient length of the inner SIMAX glass tube for the selected inner diameter.

Considering the designed range of sampled air flow rates, the calculations were performed for several flow regimes, which are summarized in Table 3.

Figure 4 presents the dependence of the total heat duty removed from the process air and the corresponding condensate production rate on the process air volumetric flow rate.

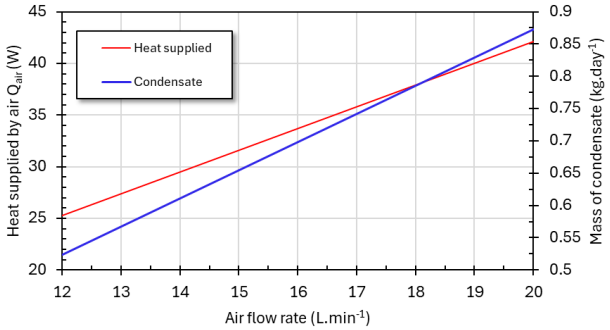

Figure 4. Dependence of heat transfer rate and condensate production on process air flow rate

Analysis of Figure 4 indicates a progressive increase in the total heat duty of the cooler, which comprises the sensible heat of dry air, the sensible heat of water vapour, and the latent heat released during condensation. As the process air flow rate increases from 12 to 20 L.min^{-1}, the total heat load rises from 25.283 W to 42.138 W, corresponding to an increase of 66.67% relative to the minimum flow rate. This trend reflects the proportional relationship between mass flow rate and the overall enthalpy change of the gas mixture.

Simultaneously, the predicted condensate production increases from 0.524 to 0.873 kg.day^{-1}. Although the absolute amount of condensate is relatively low, its accumulation inside the narrow inner tube (inner diameter 6 mm) may potentially lead to the formation of a thin liquid film on the tube wall. Such a film could locally reduce the gas-side heat transfer coefficient and slightly increase hydraulic resistance. It should be noted that these effects were not explicitly included in the present thermo-hydraulic model, which is based on overall heat balance and simplified single-phase flow assumptions for pressure drop calculation.

To ensure reliable long-term operation and to minimize the risk of local condensate accumulation and flow obstruction, the installation of a condensate collector (separator) at the cooler outlet is recommended. In addition, periodic purging of the air-side tube can be applied if necessary.

Considering the latent heat of vaporization of water (approximately 2.4 × 10^6 J.kg^{-1} in the relevant temperature range), the latent heat component represents a substantial fraction of the total heat duty. Even at the lower airflow rate, the latent contribution forms a dominant part of the overall thermal load, confirming that condensation significantly influences the required cooling capacity. Neglecting phase change effects would therefore result in an underestimation of the total heat duty and, consequently, the required heat transfer area.

This effect is directly reflected in the sizing of the cooler. Since the required heat transfer area is determined from the relationship (14) an increase in total heat duty due to latent heat release leads to a proportional increase in the required heat transfer surface S, provided that the overall heat transfer coefficient k_L and logarithmic mean temperature difference Δt_sremain within the same order of magnitude. For the given geometric constraint (inner tube diameter of 6 mm), the increase in required surface area is achieved by extending the effective length of the inner SIMAX glass tube.

At higher airflow rates, the combined effect of increased sensible heat load and intensified condensation results in a noticeable increase in the calculated exchanger length. This confirms that the latent heat contribution is a decisive design parameter for determining the optimal cooler dimensions. Therefore, accurate prediction of condensate formation is essential not only for hydraulic stability but also for reliable thermal sizing of the sample gas cooler.

To prevent flooding of the heat exchanger, periodic purging of the air-side tube is proposed.

Figure 5 shows the dependence of the required cooling water flow rate on the sampled process air flow rate at the fermenter outlet for different cooling water inlet temperature regimes (2/20 °C, 5/20 °C, 10/20 °C, 13/20 °C, and 15/20 °C).

Various inlet temperatures of the cooling water were considered in order to evaluate the influence of seasonal variations in river water temperature on the thermal and hydraulic performance of the cooler.

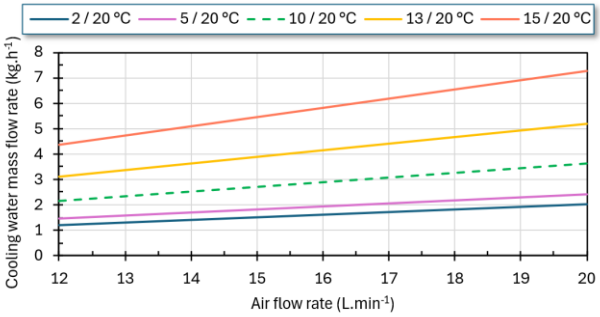

Figure 5. Cooling water flow rate as a function of process air flow rate

The dependencies shown in Figure 5 exhibit an approximately linear increase in the required cooling water flow rate with increasing process air flow rate. This trend follows directly from the heat balance of the exchanger, since the total heat duty increases proportionally with the mass flow rate of air and with the amount of water vapour undergoing condensation. For a constant cooling water temperature rise (Δt = 10 K), the higher heat load must be compensated by an increase in the cooling water mass flow rate.

Verification calculations based on the Reynolds number confirmed that, over the entire investigated operating range, the cooling water flow remains within the laminar regime. The minimum Reynolds number (Re = 10.727) was obtained for the 5/20 °C cooling water regime at the lowest process air flow rate of 12 L.min^{-1}, while the maximum value (Re = 62.113) occurred under the most demanding temperature conditions (15/20 °C) at the highest air flow rate of 20 L·min^{-1}. Despite an approximately 5.7-fold increase in Reynolds number, the flow remained clearly laminar. This ensures stable heat transfer conditions and predictable hydraulic behaviour in the cooling circuit. The selected outer tube diameter of 40 mm therefore represents a suitable compromise between sufficient heat transfer performance and acceptable pressure losses.

Since the cooling medium is assumed to be river water, relatively stable inlet temperatures can be expected under steady-state conditions throughout most of the year. Provided that the thermal balance between the incoming heat load and the heat removed by the cooling water is maintained, the system preserves the designed hydraulic regime.

From a quantitative perspective, the lowest cooling water flow rates were obtained for the 2/20 °C regime, ranging from 1.21 to 2.01 kg.h^{-1} depending on the process air flow rate. These values correspond to winter river water temperatures. Conversely, the highest flow rates were required for the 15/20 °C regime, ranging from 4.35 to 7.25 kg.h^{-1}, representing the most demanding summer conditions. In both cases, the cooling water flow rate increased by a factor of approximately 1.67 when the process air flow rate increased from its minimum to maximum value.

When comparing the influence of inlet cooling water temperature, increasing the temperature from 2 °C to 15 °C results in an approximately 3.61-fold increase in the required cooling water flow rate, corresponding to a 260.75% increase relative to the minimum case. Considering that the average annual river water temperature is close to 10 °C, the results calculated for the 10/20 °C regime can be regarded as representative of typical operating conditions. The required flow rates at this temperature lie approximately midway between the extreme winter and summer scenarios.

Figure 6 illustrates the dependence of the required cooling tube length and the corresponding distributed pressure loss on the process air flow rate. The shortest tube length corresponds to an air flow rate of 12 L.min^{-1}, the intermediate length to 16 L.min^{-1}, and the longest tube to 20 L.min^{-1}.

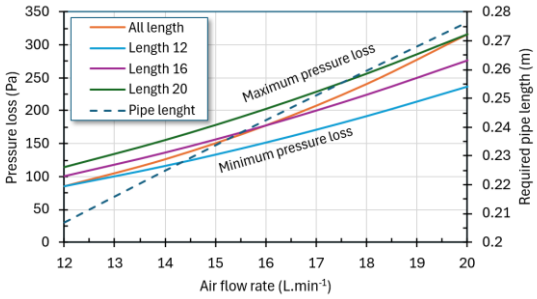

Figure 6. Effect of process air flow rate on cooling tube length and distributed pressure loss

The results presented in Figure 6 show that both the required cooling tube length and the associated distributed pressure loss increase with increasing process air flow rate. The required tube length rises from 20.68 cm at 12 L.min^{-1} to 27.66 cm at 20 L.min^{-1}, representing an increase of 33.74%. This increase reflects the higher heat duty that must be removed at elevated air flow rates.

Correspondingly, the calculated distributed pressure loss increases from 85.85 Pa to 315.77 Pa, which represents an absolute increase of 229.92 Pa. The increase in pressure loss is caused by the combined effect of higher gas velocity and greater tube length.

For the shortest tube, the pressure loss varies within a range of 150.26 Pa across the investigated flow rates, whereas for the longest tube the variation reaches 200.96 Pa. This difference (50.69 Pa) occurs at higher absolute pressure levels associated with the maximum process air flow rate.

Despite the increase in distributed pressure loss, the absolute values remain very low relative to the inlet process air pressure. Even at the maximum calculated value, the additional pressure drop introduced by the cooler does not significantly affect the transport of the sampled air to the analyzer located approximately 200 m from the sampling point.

The inner tube diameter of 8 × 1 mm (inner diameter 6 mm) was specified by the client primarily due to the required high thermal shock resistance of the SIMAX borosilicate glass and compatibility with the existing sampling line connections. Within this given geometric constraint, the required cooling tube length was determined through integrated thermo-hydraulic calculations. The resulting lengths (20.68–27.66 cm) represent an optimization outcome under the given constraints, ensuring the minimal necessary heat transfer area to achieve the target outlet air temperature across the entire range of air flow rates (12–20 L·min^{-1}) while maintaining minimized pressure drop.

This design therefore combines a client-specified parameter (tube diameter) with calculation-based optimization (tube length), resulting in a well-balanced solution that delivers excellent hydraulic performance without significant design compromises in cooling efficiency or sampling representativeness.

Overall, the results confirm that the proposed tube-in-tube counter-current heat exchanger design ensures the required thermal performance while maintaining acceptable hydraulic conditions. The combination of moderate tube length, limited condensate formation, and low pressure losses guarantees stable and reliable operation of the sampling system.

4 CONCLUSIONS

This study presented the design and thermal–hydraulic analysis of a tube-in-tube counter-current heat exchanger intended for cooling sampled process air from a fermenter prior to transport to a mass spectrometric analyzer.

The proposed configuration achieved the required outlet air temperature within a heat duty range of 25–42 W while maintaining a saturated air state, thus preventing further condensation during transport. The counter-current arrangement enabled the required performance with a compact tube length of 0.21–0.28 m.

Although the calculated daily condensate production is moderate (0.52–0.87 kg·day^{-1}), its accumulation in the narrow 6 mm inner tube could affect local flow conditions and heat transfer performance. Since the present model does not include detailed two-phase flow simulation, periodic purging of the air-side tube or installation of a condensate separator at the cooler outlet is recommended to maintain stable operation.

Depending on seasonal inlet water temperatures (2–15 °C), the required cooling water flow rate varied between 1.21 and 7.25 kg.h^{-1}, while maintaining laminar flow (Re < 63). The calculated distributed pressure losses ranged from 86 to 316 Pa, corresponding to less than 0.3% of the inlet process air pressure, and therefore do not affect sample transport over 200 m.

Overall, the proposed heat exchanger satisfies the thermal and hydraulic requirements of the sampling system and represents a compact, energy-efficient, and technically robust solution for conditioning process air prior to gas analysis.

ACKNOWLEDGMENTS

This article was supported by the Cultural and Educational Grant Agency of the Ministry of Education, Research, Development, and Youth of the Slovak Republic, through the project KEGA 024TUKE-4/2024 and the project VEGA 1/0723/25.

REFERENCES

[Chriastel 1993] Chriastel, L., Masura, S., Vavrik, E., et al. Jet loop bioreactor (JLR type) for the production of yeast biomass. Kvasny prumysl, 1993, Vol. 39, No. 1, pp. 7-9. https://doi.org/10.18832/kp1993002 (in Czech)

[Dosaev 2025] Dosaev, A.A., Safarov, R.R., Menshutina, N.V. Classification analysis of modern bioreactor systems (review). Part 1. Classification of bioreactors by design parameters. Modern Sci. and Innov., 2025,

No. 1, pp. 106-125. https://doi.org/10.37493/2307-910X.2025.1.9 (In Russian)

[Filo 2024] Filo, M., et al. Application of Unsteady Fluid Flow Simulation in the Process of Regulating an Industrial Hydraulic Network. Appl. Sci., 2024, Vol. 14, 2393, pp. 1-18. https://doi.org/10.3390/app14062393

[Gaikwad 2018] Gaikwad, V., Panghal, A., Jadhav, S., et al. Designing of Fermenter and its utilization in food industries. Preprints, 2018, 2018080433, https://doi.org/10.20944/preprints201808.0433.v1

[Hasek 1980] Hasek, P. Tables for Thermal Engineering, 11th ed., VSB: Ostrava, Czech Republic, 1980.

[KAVALIERGLASS 2018] KAVALIERGLASS, a.s. SIMAX – Industrial Apparatuses (technical catalogue), Sazava, Czech Republic, 2018 [online]. [cit. 2026-02-15]. Available from: https://www.kavalier.cz/wp-content/uploads/2025/07/1692249856_cs_catalogue_apparatuses-1.pdf

[Livansky 1989] Livansky, K. and Kajan, M. Evaluation of the Feasibility of Growing Aerobic Microorganisms in a Suspension Trickling over an Inclined Cultivation Surface. Kvasny prumysl, 1989, Vol. 35, No. 8-9, pp. 239-242. https://doi.org/10.18832/kp1989034 (in Czech)

[Paca 1987] Paca, J. Bioreactors. V. Airlift Reactors. Kvasny prumysl, 1989, Vol. 33, No. 6, pp. 176-179. https://doi.org/10.18832/kp1987037 (in Czech)

[Raznjevic 1984] Raznjevic, K. Thermodynamic Tables, 1st ed. Alfa, Bratislava, 1984.

[Rimar 2021] Rimar, M., Kizek, J., Fedak, M., Pandova, I. Utilization of RES in multivalent thermodynamic systems, 1st ed. Kosice: TUKE, 2021. ISBN 978-80-553-3884-2 (In Slovak)

[Ritonja 2021] Ritonja, J., Gorsek, A., Pecar, D. Use of a Heating System to Control the Probiotic Beverage Production in Batch Bioreactor. Appl. Sci., 2021, Vol. 11, 84. https://doi.org/10.3390/app11010084

[Shinde 2022] Shinde, A., Palake, A., Mohite, B. et al. Multi-objective Heat Sink Optimization by Using Taguchi Method. Int. J. for Research in Applied Science & Engineering Technology, 2022, Vol. 10, No. 4, pp. 2226-2232. https://doi.org/10.22214/ijraset.2022.41740

[STN ISO 3585 1998] STN ISO 3585 Borosilicate glass 3.3 — Properties, International Organization for Standardization, 1998.

[STN EN 17255-1 2020] STN EN 17255-1 Air quality. Stationary source emissions. Data acquisition and handling systems. Part 1: Specification of requirements for data handling and reporting, 2020.

[STN EN 17255-2 2021] STN EN 17255-2 Air quality. Stationary source emissions. Data acquisition and handling systems. Part 2: Specification of requirements for data acquisition and handling systems, 2021.

[STN EN 17255-3 2022] STN EN 17255-3 Air quality. Stationary source emissions. Data acquisition and handling systems. Part 3: Specification of requirements for performance testing of data acquisition and handling systems, 2022.

[STN EN 17255-4 2024] STN EN 17255-4 Air quality. Stationary source emissions. Data acquisition and handling systems. Part 4: Specification of requirements for installation and ongoing quality assurance and quality control of data acquisition and handling systems, 2024.

[Titova 2024] Titova, M., Popova, E., Nosov, A. Bioreactor Systems for Plant Cell Cultivation at the Institute of Plant Physiology of the Russian Academy of Sciences: 50 Years of Technology Evolution from Laboratory to Industrial Implications. Plants, 2024, Vol. 13, No. 3, 430. https://doi.org/10.3390/plants13030430

[Valdiani 2019] Valdiani, A., Hansen, O.K., Nielsen, U.B., et al. Bioreactor-based advances in plant tissue and cell culture: challenges and prospects. Critical Reviews in Biotechnology, 2019, Vol. 39, No. 1, pp. 20-34. https://doi.org/10.1080/07388551.2018.1489778

[Varga 2013] Varga, A., Jablonsky, G., Lukac, L., Kizek, J. Thermal technology for metallurgists, 1st ed. Kosice:TUKE, 2013. ISBN 978-80-553-1590-4 (In Slovak)

[Varga 2025a] Varga, A. Data Acquisition Systems in Emission Monitoring: EN 17255 Requirements and Practical Implementation. Adv. in Thermal Processes and Energy Transform., 2025, Vol. 8, No. 2, pp. 28-32. https://doi.org/10.54570/atpet2025/08/02/0028

[Varga 2025b] Varga, A. Deployment of the D-EMS 2020 System in a Comprehensive AMS-E Solution. Advance in Thermal Processes and Energy Transformation, 2025, Vol. 8, No. 3, pp. 39-43. https://doi.org/10.54570/atpet2025/08/03/0039

[Zajemska 2011] Zajemska, M. and Radomiak, H. The ecological and economic analysis of heat production from different fuels and wastes. Rynek Energii, 2011, Vol. 96, No. 6, pp. 33-39. ISSN 1425-5960

CONTACTS:

Prof. Ing. Miroslav Rimar, CSc.
Assoc. Prof. Ing. Jan Kizek, PhD.
Assoc. Prof. Ing. Marcel Fedak, PhD.
Assoc. Prof. Ing. Peter Oravec, CSc.
Technical University of Kosice
Faculty of Manufacturing Technologies with a seat in Presov
Department of Process Technique
Sturova 31,080 01 Presov, Slovak Republic
tel.: +421 55 602 6341; +421 55 602 6329
miroslav.rimar@tuke.sk; jan.kizek@tuke.sk;
marcel.fedak@tuke.sk; peter.oravec@tuke.sk

Dr. inz. Wojciech Bialik
Silesian University of Technology
Faculty of Materials Engineering
Krasinskiego 8, 40-019 Katowice, Poland
+48 32 603 42 21
wojciech.bialik@polsl.pl
Prof. Leonid Gres, D.Sc.
Ukrainian State University of Science and Technologies
Dnipro Metallurgical Institute
Department of Ecology, Heat Engineering, Occupational Safety and Health
Lazariana St., 2, Dnipro, 49010, Ukraine
+38095 92 455 30, leonid.gres@gmail.com